



# Facile crosslinking of poly(vinylpyrrolidone) by electro-oxidation with IrO<sub>2</sub>-based anode under potentiostatic conditions

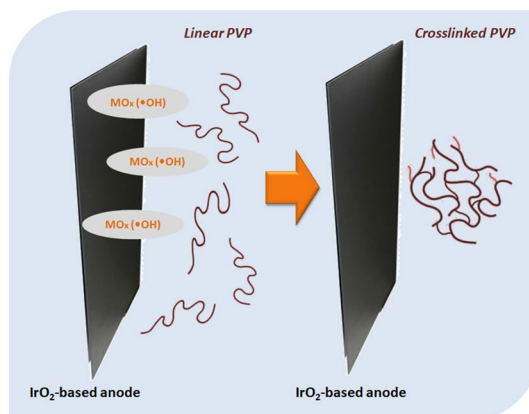
Sonia Lanzalaco<sup>1,2</sup> · Ignasi Sirés<sup>3</sup> · Alessandro Galia<sup>4</sup>  · Maria Antonietta Sabatino<sup>4</sup> · Clelia Dispenza<sup>4</sup> · Onofrio Scialdone<sup>4</sup>

Received: 27 March 2018 / Accepted: 11 July 2018  
© Springer Nature B.V. 2018

## Abstract

The modification of polymer architectures by reaction with chemically adsorbed hydroxyl radicals has been thoroughly investigated by electrolyzing dilute aqueous solutions of the biocompatible polymer poly(vinylpyrrolidone) (PVP), using an undivided electrolytic cell with a Ti/IrO<sub>2</sub>-Ta<sub>2</sub>O<sub>5</sub> (DSA<sup>®</sup>) anode. Several electrolyses were performed to assess the influence of the applied potential, the circulated charge and the PVP concentration, which was always kept low to avoid chain overlapping. From the results obtained, it can be concluded that the electro-oxidation of PVP solutions using a cheap anode is an effective method to crosslink initially isolated polymer chains, eventually increasing the size of their random coils. Furthermore, the average size of the modified macromolecules can be controlled by tuning the electrode potential and/or the current density and the circulated charge. At high anodic potential values, the hydroxyl radicals formed at DSA<sup>®</sup> were also effective to generate reactive functional groups on the PVP backbone, which is a very interesting feature for future biomedical applications.

## Graphical Abstract



**Keywords** Crosslinking · Dimensionally stable anode · Electrosynthesis · Hydroxyl radical · Nanogel · Poly(vinylpyrrolidone)

✉ Ignasi Sirés  
i.sires@ub.edu

✉ Alessandro Galia  
alessandro.galia@unipa.it

Extended author information available on the last page of the article

## 1 Introduction

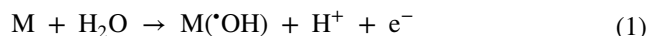
Polymer nanogels are constituted by networks of polymer chains expanded by solvent molecules that infiltrate into their pores, giving rise to nanometric structures with multiple applications [1]. They have found an essential niche

market in biomedicine [2], since biocompatible nanogels can be used as platforms to convey drug molecules [3–5] and genetic material [6, 7] in living tissues. In the particular case of delivery of agents to the brain, the presence of physiological obstacles like blood brain barrier and blood cerebrospinal fluid represents a major challenge [8]. However, nasal drug delivery technologies based on nanogels seem very adequate to address it [9, 10], thus becoming an emerging tool against Alzheimer's disease [11].

A large variety of techniques is available to induce the formation of covalent bonds within or between polymer chains, yielding nanogels whose dimensions and architecture depends on the intra/intermolecular crosslinking ratio. Many methods employ monomers to simultaneously achieve polymerization and crosslinking [12, 13] but, in some cases, bond formation from preformed polymers is also feasible [1]. In the latter case, nanogels have been prepared by physical self-assembly [3], electrospray [14], UV photoirradiation [15] and ionizing radiation (gamma rays or high-energy electrons) [16]. In aqueous media, radiation chemistry produces very reactive species like hydroxyl radicals ( $\cdot\text{OH}$ ), monoatomic H and solvated electrons, which eventually create radical sites on the polymer backbone and/or on side chains [17]. This technique is particularly advantageous because of the minimization of toxic additives [1, 17], which is crucial for biomedical purposes, along with the easy control of the reaction heat and the concomitant sterilization of the nanogel dispersion [16, 17]. Among the various polymers that may undergo crosslinking upon irradiation, poly(*N*-vinylpyrrolidone) (PVP) has attracted much attention [1, 6, 11, 18–20]. High hydrophilicity and biocompatibility along with adhesive and bonding ability and low toxicity make PVP nanogels appear as suitable candidates for diverse applications [1, 21]. For example, PVP is a key component in hydrogel wound dressings [22]. Furthermore, it is possible to produce PVP copolymers and functional PVP nanogels, as occurs upon combination with poly(acrylic) acid [23] and monoclonal antibodies [24], which increases the potentialities of this material.

Within this context, the electrochemical technology offers a promising, alternative green route for the  $\cdot\text{OH}$ -based production of high purity PVP nanogels. In particular, we have recently demonstrated for the first time the promotion of electrochemical crosslinking in aqueous PVP solutions by means of electrochemical advanced oxidation processes (EAOPs) like electro-oxidation (EO) and electro-Fenton (EF) [25, 26]. Both methods allow the generation of hydroxyl radicals on site in a controlled manner upon accurate modulation of the electrolysis conditions [27, 28]. Main operation parameters have been optimized for EF, leading to size reduction of PVP nanoparticles down to 9 nm and functionalization with  $-\text{COOH}$  and succinimide groups [26]. In contrast, the performance of EO

has not been investigated in detail yet. From an application standpoint, EO is the most appropriate EAOP since it requires simpler setups and no addition of metal catalyst, unlike EF, which favors its potential implementation. In EO, adsorbed  $\cdot\text{OH}$  is produced from water oxidation at the anode surface (M), as follows [29]:



Since hydroxyl radical on a large  $\text{O}_2$ -evolution overpotential anode like boron-doped diamond (BDD) is physically adsorbed, it becomes excessively aggressive and induces quick oxidation with promotion of bond cleavage [25]. Therefore, it is necessary to employ materials with a lower oxidation power like the so-called dimensionally stable anodes (DSA<sup>®</sup>), where  $\text{M}(\cdot\text{OH})$  is chemisorbed. This means that it mainly exists as a superoxide ( $\text{MO}$ ) and pre-eminently favors a milder reactivity with organic molecules [29, 30]. These kinds of anodes are made of metal and mixed-metal oxides [30, 31], being  $\text{IrO}_2$ -based anodes preferred for  $\text{O}_2$  evolution with  $\text{M}(\cdot\text{OH})$  as intermediate [32–38]. As a result, the attack of this species on PVP may be more controlled. Moreover, these anodes exhibit relevant technological characteristics like low cost and high durability and stability [29].

Most probably, two dominant radical structures result from  $\text{M}(\cdot\text{OH})$  attack on PVP, as shown in Fig. 1, formed via H-abstraction from the methylene and methylenide groups [17, 39]. Nonetheless, once these reactive organic radicals are generated, different reactions involving just one radical (e.g., chain scission, hydrogen transfer) or two radicals (e.g., crosslinking, disproportionation) may occur, whose extent will depend on the electrolysis conditions. This paper presents the first concise study of the influence of operation parameters on the formation of PVP nanogels from crosslinking of PVP nanoparticles with electrogenerated  $\text{M}(\cdot\text{OH})$ . Nanogels have colloidal properties and hence, the change of dimensions upon crosslinking was assessed in terms of hydrodynamic radius ( $R_h$ ) by dynamic light scattering (DLS) and gel permeation chromatography (GPC). Furthermore, the possibility of concomitant nanogel functionalization by introduction of oxygenated functional groups was analyzed by FT-IR, whereas solution mineralization was studied by total organic carbon (TOC) analysis.

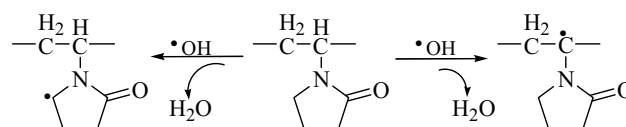


**Fig. 1** Main routes for radical formation on PVP chains from attack of  $\cdot\text{OH}$

## 2 Materials and methods

### 2.1 Reagents and electrosynthesis of polymer nanogels

The preparation of working solutions was very simple, since they were composed of double-distilled water, PVP k-60 as linear polymer ( $M_n = 1.60 \times 10^5 \text{ g mol}^{-1}$ ,  $M_w = 3.95 \times 10^5 \text{ g mol}^{-1}$ , 45 wt% solution, Aldrich) used as received, and  $\text{Na}_2\text{SO}_4$  (Aldrich) as supporting electrolyte. The concentration at which overlapping of PVP chains dissolved in water cannot be disregarded was estimated as  $\sim 1\%$  in a previous study [40]. The oxygen was stripped by purging the solutions with nitrogen (99.998% purity, Air Liquide). Membranes of 12–14 kDa cutoff (Spectrum Laboratories) and syringe filters of 1.22  $\mu\text{m}$  (Aldrich), both made of cellulose acetate, were used. KBr (FT-IR grade) needed for IR analyses and  $\text{NaN}_3$  for gel permeation chromatography (GPC) analyses were purchased from Sigma-Aldrich and Fluka, respectively.

The electro-oxidation trials were carried out in an undivided glass cell equipped with a water jacket. The desired temperature (20 °C) was kept constant by means of an Ultratemp 2000 water bath from Julabo. A fixed volume (50  $\text{cm}^3$ ) of fresh PVP aqueous solutions, stirred overnight and filtered with 0.22  $\mu\text{m}$  nylon filters under vacuum, was placed in the electrolytic cell and the experiments were performed under continuous stirring with a magnetic bar at 400 rpm to ensure fast mass transport of all reactants. This is crucial to ensure the contact between PVP chains and  $\text{M}(\cdot\text{OH})$  formed at the anode surface. A Ti/IrO<sub>2</sub>-Ta<sub>2</sub>O<sub>5</sub> (DSA<sup>®</sup>) plate from ElectroCell AB and a Ni plate were used as the anode and cathode, respectively, both presenting an exposed geometric surface area of 3  $\text{cm}^2$  and being separated about 1.0 cm from each other. SCE was used as reference electrode and all reported potential values are referred to it. An Amel 2053 potentiostat/galvanostat was employed to perform trials under potentiostatic conditions. After each experiment, the final solution was filtered with the above mentioned syringe filters and stored to perform all the analyses. All electrolyses were performed twice.

### 2.2 Analytical procedures

After each single treatment, the electrolyzed solutions were analyzed by different techniques: total organic carbon (TOC) analysis, dynamic light scattering (DLS), gel permeation chromatography (GPC) and Fourier transform infrared spectroscopy (FT-IR). The results were compared with those of the untreated solution.

To evaluate the TOC of the solution, the samples were filtered and directly injected into a Shimadzu LCSH analyzer. Scattering analyses, which are essential to understand variations of the  $R_h$  of the PVP chains, were carried out using a Brookhaven BI-9000 correlator and a 50 mW He-Ne laser (MellesGriot) tuned at  $\lambda = 532 \text{ nm}$ , and the values were compared with those of the untreated linear PVP. In particular, DLS data were analyzed according to the method of cumulants [41]. Measurements were always carried out on replicate samples, and the estimated uncertainty in the  $R_h$  values was  $\pm 20\%$ .

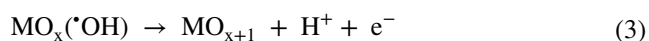
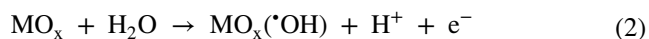
Chromatographic analyses of samples were performed with an Agilent 1100 Series HPLC, and a solution of 3  $\text{mmol dm}^{-3}$   $\text{NaN}_3$  was eluted at 0.5  $\text{cm}^3 \text{ min}^{-1}$  as mobile phase. The instrument has been equipped with two Shodex columns (804 and 806) in series, thermostated at 20 °C, and coupled to a refraction index (RI) detector at 35 °C. Prior to GPC and FT-IR analyses,  $\text{Na}_2\text{SO}_4$  was removed by dialysis in distilled water for 96 h employing cellulose acetate membranes (12 kDa cutoff). In order to assess eventual variations of the chemical structure during the treatments, infrared spectra were recorded on a Perkin-Elmer Spectrum 400. Each analysis was performed at 32 scans, with 2  $\text{cm}^{-1}$  resolution within a wavenumber range between 4000 and 400  $\text{cm}^{-1}$ . The samples were prepared by weighting amounts of nanoparticles and mixing with KBr in a mortar, followed by pressing into discs with a 10 ton pressure to obtain a film. The solid material was obtained from the aqueous solutions by freeze drying.

## 3 Results and discussion

### 3.1 Effect of PVP concentration

First experiments were performed with a commercial DSA<sup>®</sup> in an aqueous solution of PVP at 0.10 wt%, which also contained 0.05  $\text{mol dm}^{-3}$   $\text{Na}_2\text{SO}_4$  as supporting electrolyte. Potentiostatic conditions were selected, with an anodic potential of 2.2 V for a charge circulation of 750 C (resulting current of 40 mA). DSA<sup>®</sup> was chosen as the anode since higher oxidation states are available for this material. From the general reaction (1), the oxidation of water at DSA<sup>®</sup> can be interpreted according to reactions (2) and (3). This allows the formation of chemisorbed active oxygen, which is expected to promote the selective oxidation of organics like PVP without inducing a massive mineralization [25]. Therefore, in the case of preformed polymers like PVP, this could eventually induce a certain degree of crosslinking and finally give rise to the nanogels of interest. Ti/IrO<sub>2</sub>-Ta<sub>2</sub>O<sub>5</sub> was selected as a convenient example of DSA<sup>®</sup> because iridium oxide is a good catalyst to produce chemisorbed active oxygen and, in combination with Ta oxides, the overall

stability of the anode material is excellent [42]. As illustrated by reaction (4), in the absence of sufficient amount of organic molecules, chemisorbed active oxygen is expected to evolve towards oxygen [29].



As deduced from DLS data depicted in Fig. 2a, a small but noticeable increase of the  $R_h$  from about 23–27 nm was achieved upon electro-oxidation, which can be interpreted from the predominance of intermolecular crosslinking over the intramolecular modification. On the other hand, as shown in Fig. 2b, the GPC analyses reveal that the adopted electrochemical technique has two main effects: (i) the generation of a family of PVP chains with high molecular weight (detector response at times between 25.0 and 27.0 min), and (ii) the appearance and significant enhancement of two peaks characterized, respectively, by a smaller ( $\sim 37.7$  min) and a larger ( $\sim 29.6$  min) molecular weight, if compared with the untreated PVP. Hence, the electrogenerated  $\text{MO}_{x+1}$  create radical nuclei on independent PVP chains once they are able to reach the anode. Further, these macroradicals can be involved in both, intramolecular and intermolecular crosslinking, or in chain scission reactions. Furthermore, no significant variations of the TOC were detected, thus

confirming that DSA<sup>®</sup> can provide a selective modification of PVP chains without causing undesired mineralization.

To evaluate the effect of the PVP concentration, the electrolyses were repeated with a concentration of PVP of 0.25 and 0.41 wt%, as shown in Fig. 3a, b. GPC analyses of Fig. 3b show that, when the concentration of PVP was increased from 0.1 to 0.25%, the peak at about 37.7 min (associated to PVP chains with lower values of molecular weight) as well as the shoulder in the region between 25.0 and 27.0 min (related to the concentration of PVP chains with the highest molecular weights) increased remarkably. This occurred in concomitance with a decrease of the peak at  $\sim 29.6$  min. As depicted in Fig. 3a, the overall result was a higher  $R_h$  of 32 nm when operating with 0.25 wt%, probably because a larger number of PVP molecules is able to contact with the anode surface, thus favoring mainly the intermolecular crosslinking.

In contrast, when PVP concentration was further increased up to 0.41 wt% smaller modifications of both  $R_h$  and molecular weight distribution were observed. This milder crosslinking can be explained by the fact that an analogous current density, resulting in a similar rate of  $\text{MO}_{x+1}$  electrogeneration, was used for a much larger flux of PVP chains to the electrode surface. This reduces the probability of forming several radical centers in a single polymer chain and hence, many of them do not end in covalent intra/intermolecular bonding.

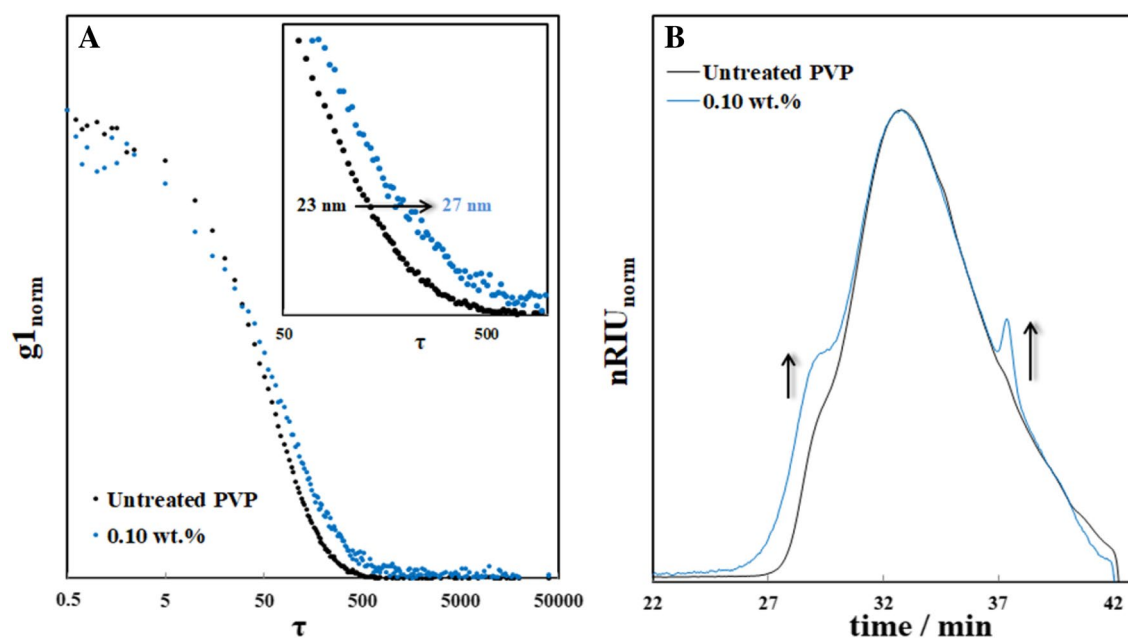


**Fig. 2** Effect of PVP crosslinking with electrogenerated  $\text{M}(\cdot\text{OH})$  using a  $\text{Ti}/\text{IrO}_2\text{-Ta}_2\text{O}_5$  anode. The electrolyses were performed with  $50 \text{ cm}^3$  of PVP at 0.10 wt% in the presence of  $0.05 \text{ mol dm}^{-3} \text{ Na}_2\text{SO}_4$

at  $20 \text{ }^\circ\text{C}$ , under potentiostatic conditions at anode potential of  $2.2 \text{ V}$  for a total charge of  $750 \text{ C}$ . DLS analysis (a) and molecular weight distribution (b) demonstrate the modifications undergone by PVP

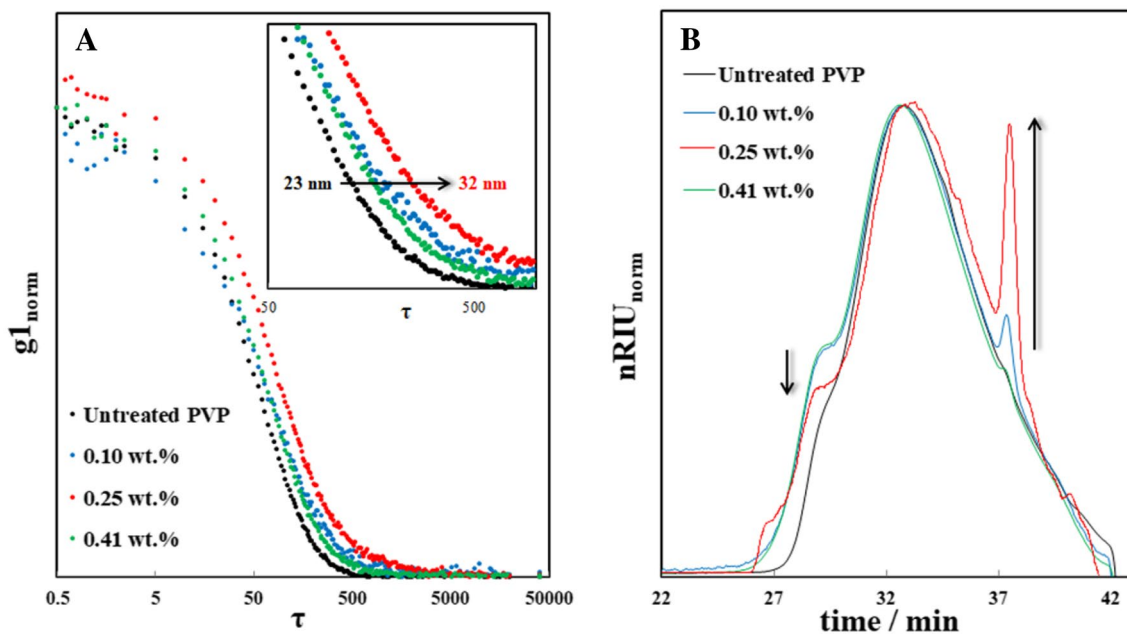


**Fig. 3** Effect of PVP concentration. DLS analysis (a) and molecular weight distribution (b) of samples obtained upon electrolyses performed with  $50 \text{ cm}^3$  of PVP, in the presence of  $0.05 \text{ mol dm}^{-3}$

$\text{Na}_2\text{SO}_4$  at  $20^\circ\text{C}$ , under potentiostatic conditions at anode potential of  $2.2 \text{ V}$  for a total charge of  $750 \text{ C}$

### 3.2 Effect of the charge consumed

In order to evaluate the effect of the charge circulated during the electrolytic trials, some experiments were performed with a concentration of PVP of  $0.25 \text{ wt}\%$  by

applying  $250$ ,  $500$  and  $750 \text{ C}$ , working with an anode potential of  $2.2 \text{ V}$ . As shown in Fig. 4, the following modifications could be observed in the GPC profiles (Fig. 4b) upon increase of the electric charge:

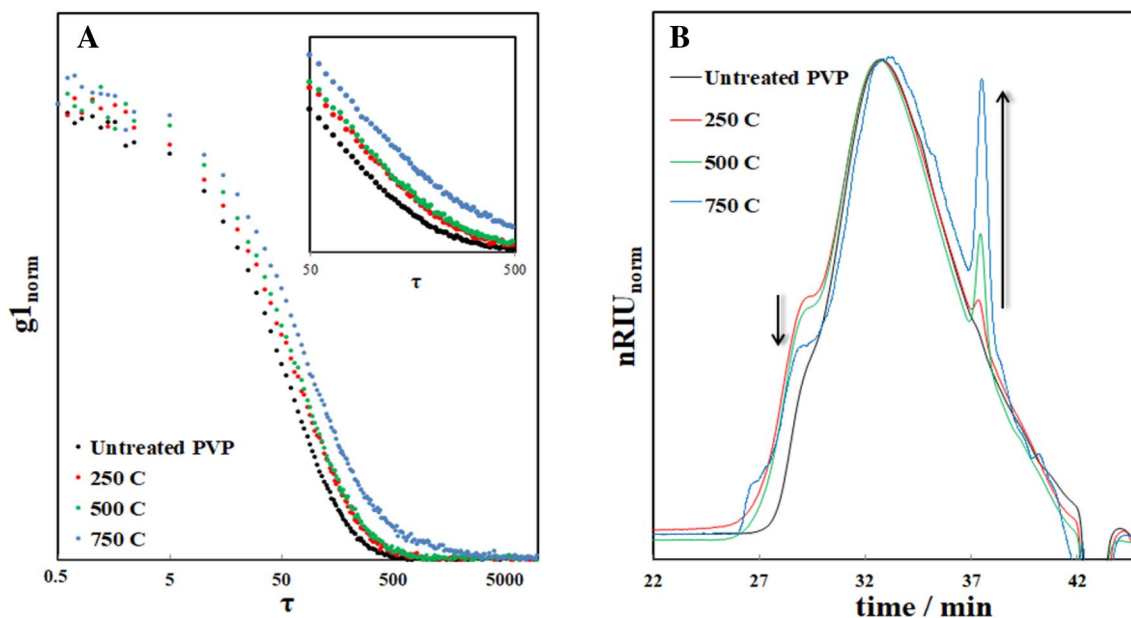


**Fig. 4** Effect of electric charge circulated under potentiostatic conditions at anode potential of  $2.2 \text{ V}$ . DLS (a) and GPC (b) analyses for the electro-oxidation of  $50 \text{ cm}^3$  of PVP at  $0.25 \text{ wt}\%$  in the presence of  $0.05 \text{ mol dm}^{-3}$   $\text{Na}_2\text{SO}_4$  at  $20^\circ\text{C}$ . Charge passed:  $250$ ,  $500$  and  $750 \text{ C}$

- (i) A progressive growth of the family of PVP coils with a quite lower molecular weight (i.e., peak at about 37.7 min in the GPC curves) was achieved as a result of the gradual prolongation of the electrochemical treatment (ending in higher circulated charges);
- (ii) A shoulder at about 29 min in Fig. 4b was clearly detectable after 250 C of circulated charge, further decreasing when the charge was increased.

These modifications in the chromatograms were accompanied by an overall increase of the  $R_h$  which was enhanced from 23 to 32 nm when the circulated charge increased from 250 to 750 C (Fig. 4a).

Hence, it can be concluded that during the anodic oxidation at a DSA<sup>®</sup> surface set at 2.2 V, various processes occur simultaneously, including both intramolecular and intermolecular crosslinking and, quite probably, chain scission. In particular, at a higher circulated charge, the intermolecular crosslinking is likely to prevail over the intramolecular one, as suggested by the enhancement of the  $R_h$ . However, this is not accompanied by a growth of molecular weight, thus evidencing partial cleavage of some fragments upon chain addition. Furthermore, it is worth observing that for all tested electric charges, the decrease of the TOC content was not significant. This demonstrates that this anode is particularly effective to induce a selective modification of the polymer without a net destruction of the macromolecules.

### 3.3 Effect of the working potential

It is well known that the performance of potentiostatic electrolysis with DSA<sup>®</sup> anodes can dramatically depend on the value of the adopted working potential [29]. In particular, the enhancement of such potential value increases the rate of  $MO_{x+1}$  electrogeneration as compared to the rate of the mass transport of the target organic to the anode surface. Therefore, it seems desirable to apply the highest potential that allows, for a given cell configuration, yielding the largest production of macroradicals upon transport of PVP toward the surface. More specifically, two limiting scenarios can be considered:

- (i) At quite low anode potential values, a very small concentration of  $MO_{x+1}$  and a relatively large concentration of PVP chains (close to the bulk concentration) are expected at the anode surface;
- (ii) At very high anode potential values, a large concentration of  $MO_{x+1}$  is expected.

In order to evaluate the effect of this parameter on the electro-oxidation process, a large set of electrolyses was performed at different values of both, the working potential (from 1.0 up to 2.5 V, resulting in current values from 3 to

50 mA) and the circulated charge (from 75 to 1500 C), using a concentration of PVP of 0.25 wt%.

In Fig. 5a, it can be observed that the effect of the circulated charge is radically different depending on the range of applied potential. At a low potential like 1.4 V, the increase of the electric charge from 75 to 250 C (i.e., equivalent to extend the electrolysis for a longer time) only caused a little change in  $R_h$ , probably due to a too slow rate of  $MO_{x+1}$  generation at the electrode solution interface. In fact, the radius became slightly smaller upon charge increase, which informs about a prevalent intramolecular crosslinking in that low potential region.

In contrast, when the anode potential was increased up to 2.2 and 2.5 V, a greater  $R_h$  with the circulated charge was observed, also finding that the rate of change increased with the anodic polarization of the electrode. Hence, at the highest studied potential of 2.5 V, the  $R_h$  was raised up to about 160 nm when the electrolysis was carried out with a circulated charge of 1500 C (Fig. 5b). This means that intermolecular crosslinking is favored within this high potential region, which can be explained from the larger number of hydroxyl radicals that lead to a higher concentration of independent macroradicals. In conclusion, this behavior indicates that electro-oxidation with DSA<sup>®</sup> can be used, unlike electro-Fenton process [26], mainly to enhance the dimensions of PVP particles, ending in more voluminous coils.

The spectroscopic investigation of the chemical structure of all fabricated polymer nanogels was carried out by FT-IR analysis. No evident oxidation of the parent chemical structure was detected, in contrast to the intensive modification observed in our previous work based on EF process [26]. This suggests that the presence and the action of  $H_2O_2$  and  $O_2$  in the EF process may contribute very significantly to the formation of oxygen-rich functional groups. In the present work, as shown in Fig. 6, only at the highest anode potential and electric charge values (i.e., 2.5 V and 1500 C) it was possible to identify a higher absorption in the 3700–3000  $cm^{-1}$  region, corresponding to the stretching of hydroxyl group and N–H stretching vibrations [43]. In addition, a mild shift and increase of the absorption at 1661  $cm^{-1}$ , related to carbonyl stretching of the pyrrolidone ring, was observed in the sample treated at 2.5 V upon circulation of 1500 C. The width of this peak also increased, if compared with the untreated PVP, most probably due to the formation of a new peak at 1695  $cm^{-1}$  associated to symmetric stretching of a cyclic imide (i.e., succinimide). This is feasible by the hydroxylation of the C atom next to the nitrogen bearing carbon of the ring [25], and here it is detected as a shoulder. Worth mentioning, the formation of such kinds of functional groups is beneficial for future functionalization of the crosslinked polymer nanoparticles, whereas it does not influence the modification process that leads to the formation of nanosized gels.

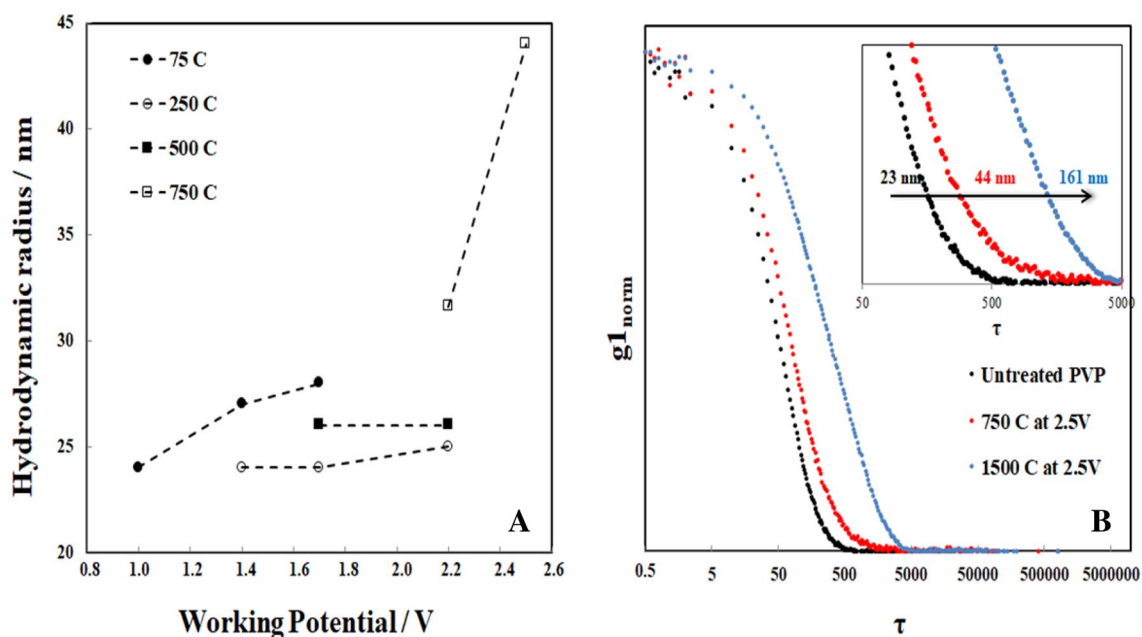
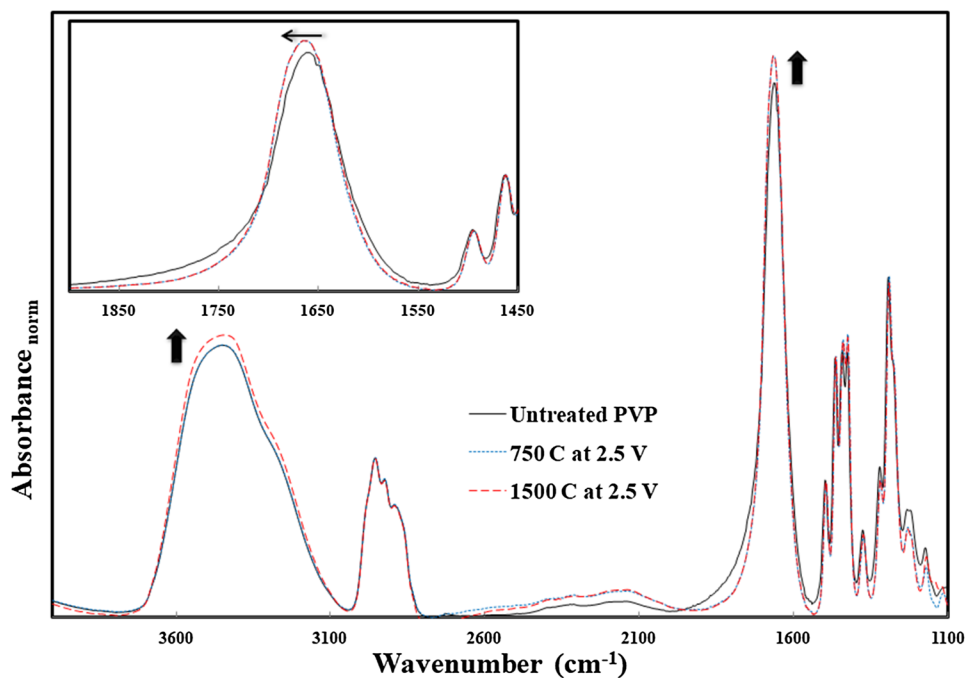


**Fig. 5** Effect of working (anode) potential. **a** Depicts the effect of the working potential on  $R_h$  during electrolyses performed with 50 cm<sup>3</sup> of PVP at 0.25 wt% in 0.05 mol dm<sup>-3</sup> Na<sub>2</sub>SO<sub>4</sub> at 20 °C, under poten-

tiostatic conditions for a total circulated charge of 75, 250, 500 or 750 C. **b** Compares the DLS analysis for trials carried out at anode potential of 2.5 V, at 750 and 1500 C

**Fig. 6** FT-IR spectra corresponding to trials treated under potentiostatic conditions for a total charge circulated of 750 or 1500 C at anode potential 2.5 V (see also Fig. 5b). The spectrum for untreated PVP is shown for comparison



### 3.4 Galvanostatic electrolyses

Since galvanostatic electrolysis mode is simpler and more suitable for scaling up of PVP nanogel electrosynthesis as compared to potentiostatic one, some electrolyses were carried out at a constant current of 15 mA for 7 h,

corresponding to a circulated charge of about 400 C. The effect of the PVP concentration was investigated within the range from 0.10 to 0.50% (w/w). In all these experiments, the electrochemical process resulted in a drastic increase of  $R_h$ . At a concentration of 0.1 wt%, the  $R_h$  increased from about 23–24 to 83.0 nm (Table 1, entries 1 and 2).

**Table 1** Effect of PVP concentration during galvanostatic electrolyses performed at 15 mA using 50 cm<sup>3</sup> of polymer solution in 0.05 mol dm<sup>-3</sup> Na<sub>2</sub>SO<sub>4</sub>, at room temperature, for a circulated charge of 391 C

Entry <sup>a</sup>	[PVP] (wt%)	I (mA)	t (s)	(Charge circulated/theoretical charge) ratio			R <sub>h</sub> (nm)	TOC decay (%)
				Mineralization <sup>b</sup>	1 H per monomeric unit <sup>c</sup>	1 H per chain <sup>d</sup>		
1	Untreated PVP						23.7	
2	0.10	15	26,013	0.264	8.97	12939.1	83.0	< 1
3	0.25	15	26,013	0.1056	3.59	5175.6	117.0	< 1
4	0.50	15	26,013	0.0528	1.79	2587.8	50.0	< 1

<sup>a</sup>All experiments were performed with 0.05 mol dm<sup>-3</sup> Na<sub>2</sub>SO<sub>4</sub>, at 20 °C

<sup>b</sup>Theoretical charge is that needed for the complete mineralization of PVP

<sup>c</sup>Theoretical charge refers to the abstraction of 1 H atom per each monomeric unit

<sup>d</sup>Theoretical charge refers to the abstraction of 1 H atom per each polymer chain

A further enhancement of  $R_h$  up to 117.0 nm (Table 1, entry 3) was obtained upon increase of PVP concentration to 0.25 wt%, suggesting that the presence of a larger number of PVP chains favors intermolecular crosslinking. However, when the concentration of PVP was further enhanced up to 0.5 wt%, a marked reduction of  $R_h$  down to about 50 nm (Table 1, entry 4) was found. This latter result is likely due to the fact that too many PVP chains are present for the adopted value of the circulated charge, thus resulting in a lower number of PVP chains bearing radical centers as well as in smaller modifications of PVP, as compared to those achieved under the other conditions. FT-IR analyses were carried out also on samples treated under galvanostatic conditions, but no evidence of changes in functional groups was observed (data not reported).

## 4 Conclusions

Aqueous solutions of PVP, at low concentration to prevent overlapping, were electro-oxidized using a Ti/IrO<sub>2</sub>-Ta<sub>2</sub>O<sub>5</sub> anode. We found that the electrogenerated MO<sub>x+1</sub> species can create radical centers on independent PVP chains that reach the DSA<sup>®</sup> surface. As a result, the activated polymer chains evolve following intramolecular and intermolecular crosslinking, or may undergo chain scissions without any significant mineralization of the polymer. The experimental results suggest that, among the various aforementioned elemental reactions, potentiostatic electro-oxidation with DSA<sup>®</sup> mainly promotes intermolecular crosslinking. As a crucial outcome, the average size of the modified macromolecules can be controlled by tuning the electrode potential and the circulated charge. In conclusion, the IrO<sub>2</sub>-based DSA<sup>®</sup> is an effective and low cost electrode to generate large polymer coils starting from preformed polymer chains.

**Acknowledgements** The authors thank Università di Palermo for support under project FR 2012/13 ID 2014-ATE-0054.

## References

- Kadlubowski S (2014) Radiation-induced synthesis of nanogels based on poly(*N*-vinyl-2-pyrrolidone): a review. *Radiat Phys Chem* 102:29–39. <https://doi.org/10.1016/j.radphyschem.2014.04.016>
- Ramos J, Forcada J, Hidalgo-Alvarez R (2014) Cationic polymer nanoparticles and nanogels: from synthesis to biotechnological applications. *Chem Rev* 114:367–428. <https://doi.org/10.1021/cr3002643>
- Kabanov AV, Vinogradov SV (2009) Nanogels as pharmaceutical carriers: finite networks of infinite capabilities. *Angew Chem Int Ed* 48:5418–5429. <https://doi.org/10.1002/anie.200900441>
- Du JZ, Sun TM, Song WJ, Wu J, Wang J (2010) Tumor-acidity-activated charge-conversional nanogel as an intelligent vehicle for promoted tumoral-cell uptake and drug delivery. *Angew Chem Int Ed* 49:3621–3626. <https://doi.org/10.1002/anie.200907210>
- Chacko RT, Ventura J, Zhuang J, Thayumanavan S (2012) Polymer nanogels: a versatile nanoscopic drug delivery platform. *Adv Drug Deliv Rev* 64:836–851. <https://doi.org/10.1016/j.addr.2012.02.002>
- Dispenza C, Adamo G, Sabatino MA, Grimaldi N, Bulone D, Bondi ML, Rigogliuso S, Ghersi G (2014) Oligonucleotides-decorated-poly(*N*-vinyl pyrrolidone) nanogels for gene delivery. *J Appl Polym Sci* 131:39974. <https://doi.org/10.1002/app.39774>
- Shatsberg Z, Zhang X, Ofek P, Malhotra S, Krivitsky A, Scomparin A, Tiram G, Calderón M, Haag R, Satchi-Fainaro R (2016) Functionalized nanogels carrying an anticancer microRNA for glioblastoma therapy. *J Control Release* 239:159–168. <https://doi.org/10.1016/j.jconrel.2016.08.029>
- Nainwal N (2017) Recent advances in transcranial focused ultrasound (FUS) triggered brain delivery. *Curr Drug Targets* 18:1225–1232. <https://doi.org/10.2174/1389450117666161222160025>
- Khan AR, Liu M, Khan MW, Zhai G (2017) Progress in brain targeting drug delivery system by nasal route. *J Control Release* 268:364–389. <https://doi.org/10.1016/j.jconrel.2017.09.001>
- Picone P, Sabatino MA, Ditta LA, Amato A, San Biagio PL, Mulè F, Giacomazza D, Dispenza C, Di Carlo M (2018) Nose-to-brain delivery of insulin enhanced by a nanogel carrier. *J Control Release* 270:23–36. <https://doi.org/10.1016/j.jconrel.2017.11.040>

11. Picone P, Ditta LA, Sabatino MA, Militello V, San Biagio PL, Di Giacinto ML, Cristaldi L, Nuzzo D, Dispenza C, Giacomazza D, Di Carlo M (2016) Ionizing radiation-engineered nanogels as insulin nanocarriers for the development of a new strategy for the treatment of Alzheimer's disease. *Biomaterials* 80:179–194. <https://doi.org/10.1016/j.biomaterials.2015.11.057>
12. Sansona N, Rieger J (2010) Synthesis of nanogels/microgels by conventional and controlled radical crosslinking copolymerization. *Polym Chem* 1:965–977. <https://doi.org/10.1039/C0PY00010H>
13. Lanzalaco S, Armelin E (2017) Poly(*N*-isopropylacrylamide) and copolymers: a review on recent progresses in biomedical applications. *Gels* 3:36. <https://doi.org/10.3390/gels3040036>
14. Chen J, Dai H, Lin H, Tu K, Wang H, Wang LQ (2016) A new strategy based on electrospray technique to prepare dual-responsive poly(ether urethane) nanogels. *Colloids Surf B* 141:278–283. <https://doi.org/10.1016/j.colsurfb.2016.01.051>
15. Chen W, Hou Y, Tu Z, Gao L, Haag R (2017) pH-degradable PVA-based nanogels via photo-crosslinking of thermopreincuded nanoaggregates for controlled drug delivery. *J Control Release* 259:160–167. <https://doi.org/10.1016/j.jconrel.2016.10.032>
16. Ulański P, Janik I, Rosiak JM (1998) Radiation formation of polymeric nanogels. *Radiat Phys Chem* 52:289–294. [https://doi.org/10.1016/S0969-806X\(98\)00155-8](https://doi.org/10.1016/S0969-806X(98)00155-8)
17. Dispenza C, Spadaro G, Jonsson M (2016) Radiation engineering of multifunctional nanogels. *Top Curr Chem (Z)* 374:69. <https://doi.org/10.1007/s41061-016-0075-6>
18. Na JC, Weaver A, Kim B, Barkatt A, Poster D, Vreeland WN, Silverman J, Al-Sheikhly M (2011) Radiation-induced synthesis of poly(vinylpyrrolidone) nanogel. *Polymer* 52:5746–5755. <https://doi.org/10.1016/j.polymer.2011.09.056>
19. Dispenza C, Grimaldi N, Sabatino MA, Todaro S, Bulone D, Giacomazza D, Przybytniak G, Alessi S, Spadaro G (2012) Studies of network organization and dynamics of e-beam crosslinked PVPs: from macro to nano. *Radiat Phys Chem* 81:1349–1353. <https://doi.org/10.1016/j.radphyschem.2011.11.057>
20. Dispenza C, Sabatino MA, Grimaldi N, Mangione MR, Walo M, Murugan E, Jonsson M (2016) On the origin of functionalization in one-pot radiation synthesis of nanogels from aqueous polymer solutions. *RSC Adv* 6:2582–2591. <https://doi.org/10.1039/C5RA23926E>
21. Teodorescu M, Bercea M (2015) Poly(vinylpyrrolidone): a versatile polymer for biomedical and beyond medical applications. *Polym Plast Technol Eng* 54:923–943. <https://doi.org/10.1080/03602559.2014.979506>
22. Rosiak JM, Yoshii F (1999) Hydrogels and their medical applications. *Nucl Instrum Methods Phys Res B* 151:56–64. [https://doi.org/10.1016/S0168-583X\(99\)00118-4](https://doi.org/10.1016/S0168-583X(99)00118-4)
23. Ghaffarlou M, Sütökin SD, Güven O (2018) Preparation of nanogels by radiation-induced cross-linking of interpolymer complexes of poly(acrylic acid) with poly(vinyl pyrrolidone) in aqueous medium. *Radiat Phys Chem* 142:130–136. <https://doi.org/10.1016/j.radphyschem.2017.04.019>
24. Adamo G, Grimaldi N, Sabatino MA, Walo M, Dispenza C, Ghersi G (2017) E-beam crosslinked nanogels conjugated with monoclonal antibodies in targeting strategies. *Biol Chem* 398:277–287. <https://doi.org/10.1515/hsz-2016-0255>
25. Galia A, Lanzalaco S, Sabatino MA, Dispenza C, Scialdone O, Sirés I (2016) Crosslinking of poly(vinylpyrrolidone) activated by electrogenerated hydroxyl radicals: a first step towards a simple and cheap synthetic route of nanogel vectors. *Electrochem Commun* 62:64–68. <https://doi.org/10.1016/j.elecom.2015.12.005>
26. Lanzalaco S, Sirés I, Sabatino MA, Dispenza C, Scialdone O, Galia A (2016) Synthesis of polymer nanogels by electro-Fenton process: investigation of the effect of main operation parameters. *Electrochim Acta* 246:812–822. <https://doi.org/10.1016/j.electacta.2017.06.097>
27. Brillas E, Sirés I, Oturan MA (2009) Electro-Fenton process and related electrochemical technologies based on Fenton's reaction chemistry. *Chem Rev* 109:6570–6631. <https://doi.org/10.1021/cr900136g>
28. Martínez-Huitle CA, Rodrigo MA, Sirés I, Scialdone O (2015) Single and coupled electrochemical processes and reactors for the abatement of organic water pollutants: a critical review. *Chem Rev* 115:13362–13407. <https://doi.org/10.1021/acs.chemrev.5b00361>
29. Panizza M, Cerisola G (2009) Direct and mediated anodic oxidation of organic pollutants. *Chem Rev* 109:6541–6569. <https://doi.org/10.1021/cr9001319>
30. Wu W, Huang ZH, Lim TT (2014) Recent development of mixed metal oxide anodes for electrochemical oxidation of organic pollutants in water. *Appl Catal A* 480:58–78. <https://doi.org/10.1016/j.apcata.2014.04.035>
31. Silva LM, Dos Santos RPA, Moraes CCO, Vasconcelos CL, Martínez-Huitle CA, Castro SSL (2017) Anodic oxidation of the insecticide imidacloprid on mixed metal oxide (RuO<sub>2</sub>-TiO<sub>2</sub> and IrO<sub>2</sub>-RuO<sub>2</sub>-TiO<sub>2</sub>) anodes. *J Electrochem Soc* 164:E489–E495. <https://doi.org/10.1149/2.1871713jes>
32. Scialdone O, Randazzo S, Galia A, Filardo G (2009) Electrochemical oxidation of organics at metal oxide electrodes: the incineration of oxalic acid at IrO<sub>2</sub>-Ta<sub>2</sub>O<sub>5</sub> (DSA-O<sub>2</sub>) anode. *Electrochim Acta* 54:1210–1217. <https://doi.org/10.1016/j.electacta.2008.08.064>
33. Scialdone O, Galia A, Randazzo S (2011) Oxidation of carboxylic acids in water at IrO<sub>2</sub>-Ta<sub>2</sub>O<sub>5</sub> and boron doped diamond anodes. *Chem Eng J* 174:266–274. <https://doi.org/10.1016/j.cej.2011.09.016>
34. Da Silva AJC, dos Santos EV, de Oliveira Moraes CC, Martínez-Huitle CA, Castro SSL (2013) Electrochemical treatment of fresh, brine and saline produced water generated by petrochemical industry using Ti/IrO<sub>2</sub>-Ta<sub>2</sub>O<sub>5</sub> and BDD in flow reactor. *Chem Eng J* 233:47–55. <https://doi.org/10.1016/j.cej.2013.08.023>
35. Cuevas O, Herrada RA, Corona JL, Olvera MG, Sepúlveda-Guzmán S, Sirés I, Bustos E (2016) Assessment of IrO<sub>2</sub>-Ta<sub>2</sub>O<sub>5</sub>/Ti electrodes for the electrokinetic treatment of hydrocarbon-contaminated soil using different electrode arrays. *Electrochim Acta* 208:282–287. <https://doi.org/10.1016/j.electacta.2016.05.045>
36. Fan Y, Cheng X (2016) Porous IrO<sub>2</sub>-Ta<sub>2</sub>O<sub>5</sub> coating modified with carbon nanotubes for oxygen evolution reaction. *J Electrochem Soc* 163:E209–E215. <https://doi.org/10.1149/2.0021608jes>
37. Herrada RA, Medel A, Manríquez F, Sirés I, Bustos E (2016) Preparation of IrO<sub>2</sub>-Ta<sub>2</sub>O<sub>5</sub>/Ti electrodes by immersion, painting and electrophoretic deposition for the electrochemical removal of hydrocarbons from water. *J Hazard Mater* 319:102–110. <https://doi.org/10.1016/j.jhazmat.2016.02.076>
38. Steter JR, Brillas E, Sirés I (2016) On the selection of the anode material for the electrochemical removal of methylparaben from different aqueous media. *Electrochim Acta* 222:1464–1474. <https://doi.org/10.1016/j.electacta.2016.11.125>
39. Spinks JWT, Woods RJ (1990) An introduction to radiation chemistry. Wiley, New York
40. Dispenza C, Ricca M, LoPresti C, Battaglia G, La Valle M, Giacomazza D, Bulone D (2011) E-beam irradiation and UV photocrosslinking of microemulsion-laden poly(*N*-vinyl-2-pyrrolidone) hydrogels for “in-situ” encapsulation of volatile hydrophobic compounds. *Polym Chem* 2:192–202. doi. <https://doi.org/10.1039/C0PY00161A>
41. Koppel DE (1972) Analysis of macromolecular polydispersity in intensity correlation spectroscopy: the method of cumulants. *J Chem Phys* 57:4814–4820. <https://doi.org/10.1063/1.1678153>

42. Ardizzone S, Trasatti S (1996) Interfacial properties of oxides with technological impact in electrochemistry. *Adv Colloid Interface Sci* 64:173–251. [https://doi.org/10.1016/0001-8686\(95\)00286-3](https://doi.org/10.1016/0001-8686(95)00286-3)
43. Grimaldi N, Sabatino MA, Przybytniak G, Kaluska I, Bondi ML, Bulone D, Alessi S, Spadaro G, Dispenza C (2014) High-energy radiation processing, a smart approach to obtain PVP-graft-AA nanogels. *Radiat Phys Chem* 94:76–79. <https://doi.org/10.1016/j.radphyschem.2013.04.012>

## Affiliations

Sonia Lanzalaco<sup>1,2</sup> · Ignasi Sirés<sup>3</sup> · Alessandro Galia<sup>4</sup>  · Maria Antonietta Sabatino<sup>4</sup> · Clelia Dispenza<sup>4</sup> · Onofrio Scialdone<sup>4</sup>

<sup>1</sup> Departament d'Enginyeria Química, EEBE, Universitat Politècnica de Catalunya, C/Eduard Maristany, 10-14, Ed. I2, Barcelona, Spain

<sup>2</sup> Barcelona Research Center in Multiscale Science and Engineering, Universitat Politècnica de Catalunya, C/Eduard Maristany, 10-14, Ed. I2, Barcelona, Spain

<sup>3</sup> Laboratori d'Electroquímica dels Materials i del Medi Ambient, Departament de Química Física, Facultat de

Química, Universitat de Barcelona, Martí i Franquès 1-11, 08028 Barcelona, Spain

<sup>4</sup> Dipartimento dell'Innovazione Industriale e Digitale (DIID), Ingegneria Chimica, Gestionale, Informatica, Meccanica, Università degli Studi di Palermo, Viale delle Scienze, 90128 Palermo, Italy